ELSEVIER

Journal of Molecular Catalysis A: Chemical 192 (2003) 171–187

JOURNAL OF MOLECULAR CATALYSIS A: CHEMICAL

www.elsevier.com/locate/molcata

Conversion of *sec*-butylbenzene over H-beta zeolites

I. Ferino, D. Meloni, R. Monaci, E. Rombi, V. Solinas*

Dipartimento di Scienze Chimiche, Università di Cagliari, Complesso Universitario di Monserrato, S.S. 554 Bivio per Sestu, 09042 Cagliari, Italy

Received 5 July 2002; accepted 9 July 2002

Abstract

The influence of pressure and temperature on the catalytic behaviour of H-beta zeolites in the conversion of *sec*-butylbenzene, an hydrocarbon present in reformed gasoline, has been investigated. The reaction pathway involves many parallel and/or successive steps, the main reactions being dealkylation, isomerization and disproportionation. The activity and stability of the catalyst increase with increasing pressure. Products distribution is also affected by pressure. An increase in temperature leads to an increase in both conversion and selectivity to dealkylation. The disproportionation and isomerization products are favoured at low temperatures. A general scheme of the process is proposed on the basis of the structural and acidic features of the catalyst.

Keywords: Beta zeolite; *sec*-Butylbenzene; Acidity; Reaction mechanism; Deactivation by coking

1. Introduction

Beta zeolite (BEA) is one of the few high-silica zeolites having a three-dimensional structure with stacking disorder. The framework structure of beta zeolite is characterized by three mutually intersecting 12-member ring (12 MR) channel systems [1,2]. Two topological identical linear channel systems are mutually orthogonal and perpendicular to the [0 0 1] plane; the pore openings of these channels are approximately 6.4 Å × 7.6 Å. A third 12-member ring channel (5.5 Å × 5.5 Å) is nonlinear and parallel to the *c*-axis; this tortuous channel system is formed by the intersection of the two linear channel systems. In a ^{129}Xe NMR study, Benslama et al. [3] had revealed that the channel intersections of beta zeolite generate cavities whose sizes are in the order of 12–13 Å. It can be synthesized within a large range of silica-to-alumina ratio (12–200) [4]. This zeolite may offer interesting opportunities as a catalyst, since it combines three important characterictics: large pores, high Si/Al synthesis ratio, and a tridirectional network of pores. In addition, the dimensions of one type of pores (5.5 Å × 5.5 Å) can originate shape selectivity effects [5].

Over acidic zeolites, alkylaromatics can undergo isomerisation (ISO), dealkylation (DEA), and disproportionation (DIS) reactions in various ratios, depending on the concentration and strength of the acid sites, on the structure of the sample and on the reaction conditions [6]. In a previous paper from this laboratory the simultaneous occurrence of these reactions in the case of *sec*-butylbenzene (sBB) conversion over HY, HMOR and HZSM-5 zeolites under atmospheric pressure has been reported [7,8]. Among the reaction products, *iso*-butylbenzene is the most

* Corresponding author. Tel.: +39-70-6754384; fax: +39-70-6754388.
E-mail address: solinas@unica.it (V. Solinas).

1381-1169/02/$ – see front matter © 2002 Elsevier Science B.V. All rights reserved.
PII: S1381-1169(02)00411-9

interesting one, being an important key-intermediate for the preparation of ibuprofen, a drug with pharmacological properties similar to those of aspirin [9].

In the present paper, the conversion of *sec*-butylbenzene (sBB) has been studied over three H-beta zeolites of different Si/Al ratio. To investigate the possibility of increasing the catalyst activity and selectivity, the sBB conversion was carried out under both atmospheric pressure and 40 bar. All the catalyst samples were characterised by N_2 adsorption–desorption for the textural features; the concentration and strength of the acid sites were assessed by means of adsorption microcalorimetry and infrared spectroscopy (FTIR) using pyridine as a probe molecule.

2. Experimental

2.1. Catalyst preparation and characterization

The sBB was a >99% pure Fluka "purum" reactant. Three H-beta zeolites with total Si/Al ratios of 17, 22 and 27 (B-17, B-22, B-27) were synthesised according to the Mobil patents [10,11]. The chemical composition was determined by elemental analysis (LIBERTY 200 ICP, VARIAN). Their apparent cristallinity was estimated by X-ray diffraction (SEIFERT). The porosity of each sample was determined by nitrogen adsorption–desorption at 77 K. A Tian-Calvet heat flow calorimeter (Setaram) equipped with a volumetric vacuum line was used for microcalorimetric measurements [12]. Each sample (100 mg) was pretreated overnight at 673 K under vacuum (10^{-3} Pa). Adsorption was carried out at 423 K by admitting successive doses of probe molecule and recording the thermal effect. The run was stopped at a final pressure of 133.3 Pa. After outgassing (10^{-3} Pa) for 1 h at 423 K, a second adsorption was carried out. From the difference between the two parallel adsorption isotherms, the concentration of irreversibly chemisorbed species was evaluated. For FTIR characterisation, the pure zeolites were pressed into thin wafers (5–15 mg/cm^2) and activated in situ in the IR cell. The activation conditions were the following: under air flow (1 cm^3/s) at 773 K for 16 h and then under vacuum (10^{-6} Torr) at 673 K for 1 h. An excess of pyridine was adsorbed at 423 K, and after 15 min of contact, physisorbed pyridine was removed by evacuation for 1 h at the same temperature. A NICOLET MAGNA IR 550 spectrometer was used for recording the spectra.

2.2. Catalyst testing

Catalytic runs were carried out in a continuous flow fixed bed stainless steel microreactor at T = 473–573 K, P = 1–40 bar and contact time τ = 0.2 $g_{cat}h/g_{sBB\,fed}$. The catalyst was activated overnight in situ at 773 K under air flow, dried before reaction and cooled down to the reaction temperature in N_2. For testing under atmospheric pressure, N_2 was used as carrier gas (N_2/sBB = 1.4–12.5 mol/mol). For runs at 40 bar, N_2 was stopped after pressurization at the desired pressure and the reactant was fed to the reactor. Samples of the effluent were collected in closed vials at 213 K to minimize the loss of lighter products and analysed on-line by a FID HP-5890 gas-chromatograph, equipped with a fused silica capillary column SUPELCO Petrocol DH 0.25 mm o.d. and 100 m long. GC–MS identification of the various products was performed on a HP-5989A apparatus. Due to the operating procedure, the fluodynamic regime was reached, in the case of high pressure, after 1 h on-stream.

3. Results

3.1. Structural and textural features

The percentage of crystallinity (CRX), estimated from the intensities of the three XRD peaks corresponding to the tetragonal system (Miller indexes: 004 around 2θ = 13.4°, 302 around 2θ = 22.4°, 008 around 2θ = 27.1°) [13], was 95, 99 and 100% for B-17, B-22 and B-27, respectively.

A typical nitrogen adsorption–desorption isotherm at 77 K is shown in Fig. 1. The microporous character of all the samples is revealed by the steep rise of the adsorbed volume (V) at very low p/p_0, followed by a plateau for p/p_0 values between 0.05 and 0.5. The presence of an hysteresis loop in the adsorption–desorption curves, typical of the presence of mesopores, is also observed at $p/p_0 = 0.45$. The diameter of these mesopores estimated by the Horvath–Kawazoe equation [14] was around 2.6 nm. Most likely, mesoporosity is related to the intercristalline voids resulting from

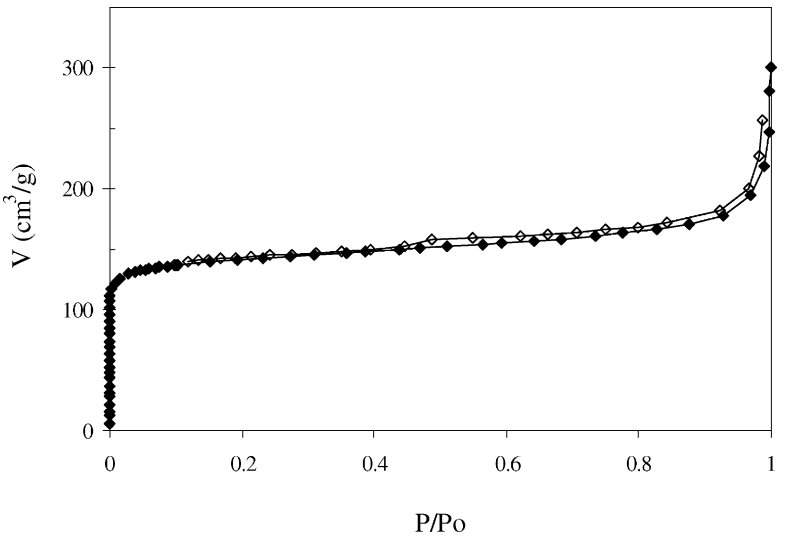

Fig. 1. Nitrogen adsorption–desorption isotherm at 77 K for B-17 sample of beta zeolite.

agglomeration of the very small cristallites of H-beta catalysts [13]. To obtain a quantitative assessment of the sample porosity, nitrogen isotherms were analysed by the Dubinin–Radushkevich (DR) equation [15]. The DR plots ($\log V$ versus $\log 2p/p_0$) were found to be linear in the range $0.04 < p/p_0 < 0.006$. The micropore capacities obtained by back extrapolation of these plots, (V_{DR}), are given in Table 1. In the same table, the total pore volume (V_{tot}) is also reported.

The *t*-plot method, based on the Harkins–Jura equation [16], was also used to analyse the adsorption data. The occurrence of a positive intercept, of a breakdown point at *t* about 4 Å and of two well-defined linear ranges, indicates the existence of different types of micropores. The total micropore volume V_t (pore diameter < 20 Å) was obtained by back extrapolation of the linear part of the *t*-plot for a thickness range lower than 10 Å [17]. The first linear range in *t*-plots did not pass though the origin, although it includes values determined at p/p_0 as low as 0.01. This indicates the presence of ultramicropores (pore diameter < 7 Å), most likely the micropores of the zeolite (5.5 Å × 5.5 Å and 6.4 Å × 7.6 Å). The total pore volume, the total volume of the micropores given by the *t*-plot methods (V_t), the ultramicropore volume (V_u) as well as the differences $V_t - V_u$ and $V_{total} - V_t$ which correspond to the volumes of the supermicropores (7 Å < pore diameter < 20 Å) and of the mesopores, respectively are reported in Table 1.

A good agreement is found between V_{DR} and V_t. For the three samples, the ultramicropore volume corresponds to 34–38% of the total pore volume, the supermicropore volume to 14–20% and the mesopore volume to 43–52%.

Table 1
Main physicochemical properties of the H-beta zeolites. Specific surface area (SA), total pore volume (V_{tot}), total micropore volume given by the Dubinin–Radushkevich (V_{DR}) and by *t*-plot methods (V_t), ultramicropore volume (V_u), supermicropores volume (V_s) and mesopore volume ($V_{meso} = V_{tot} - V_t$)

Sample	Total Si/Al[a]	SA (m^2/g)	V_{tot} (cm^3/g)	V_{DR} (cm^3/g)	V_t (cm^3/g)	V_u (cm^3/g)	V_s (cm^3/g)	V_{meso} (cm^3/g)
B-17	17.1	600	0.433	0.213	0.210	0.148	0.062	0.227
B-22	21.6	605	0.374	0.215	0.214	0.137	0.077	0.160
B-27	26.7	601	0.377	0.213	0.210	0.142	0.068	0.167

[a] From elemental analysis.

The ultramicropore volume is virtually the same for the three samples, while there is a decrease (ca. 30%) in the volume of mesopores from B-17 to B-27. The lower intercristalline volume of B-22 and B-27 is probably due to formation of more dense agglomerates of cristallites [13,18].

3.2. Acid properties

Calorimetric results for pyridine adsorption are summarized in Fig. 2 where the differential heats of adsorption (Q_{diff}) are plotted versus the pyridine uptake (n). The total pyridine uptake is in the order B-17 > B-22 > B-27. Microcalorimetric experiments reveal the presence of very strong acid sites: with B-22 and B-27, the initial value of Q_{diff} is 210 and 220 kJ/mol, respectively, whereas with B-17 it is equal to 230 kJ/mol.

The energy distribution plots $-dn/dQ_{diff}$ versus Q_{diff}, obtained by graphical derivation of the curves of Fig. 2, are shown in Fig. 3. The presence of peaks in such plots reveals the existence on the catalyst of different sets of sites, each set being homogeneous as to the strength. Different regions of Q_{diff} can be individuated. The region with Q_{diff} >135 kJ/mol is characterized for the three zeolites by the presence of a sharp peak. The region with Q_{diff} between 135 and 110 kJ/mol contains a big peak in the case of B-17, which is not present for two other catalysts. The region with Q_{diff} between 110 and 90 kJ/mol corresponds to the last portion of acid sites still able to adsorb pyridine irreversibly. The interaction with the acid sites is reversible and nonspecific below 90 kJ/mol. Accordingly, the region with Q_{diff} < 90 kJ/mol is not considered in the following. The concentration of sites of each of the three regions, indicated as n_s (Q_{diff} > 135 kJ/mol, strong), n_m (110 < Q_{diff} < 135 kJ/mol, medium), and n_w (90 < Q_{diff} < 110 kJ/mol, weak), is reported in Table 2.

Table 2
Strong (n_s: Q_{diff} > 135 kJ/mol), medium (n_m: 135 < Q_{diff} < 110 kJ/mol) and weak (n_w: 110 < Q_{diff} < 90 kJ/mol) concentrations of acid sites determined by microcalorimetry

Sample	n_s (μmol/g)	n_m (μmol/g)	n_w (μmol/g)
B-17	103	390	214
B-22	238	48	84
B-27	95	92	50

Information about the nature of the acid sites has been obtained by FTIR. The results are summarized in Table 3.

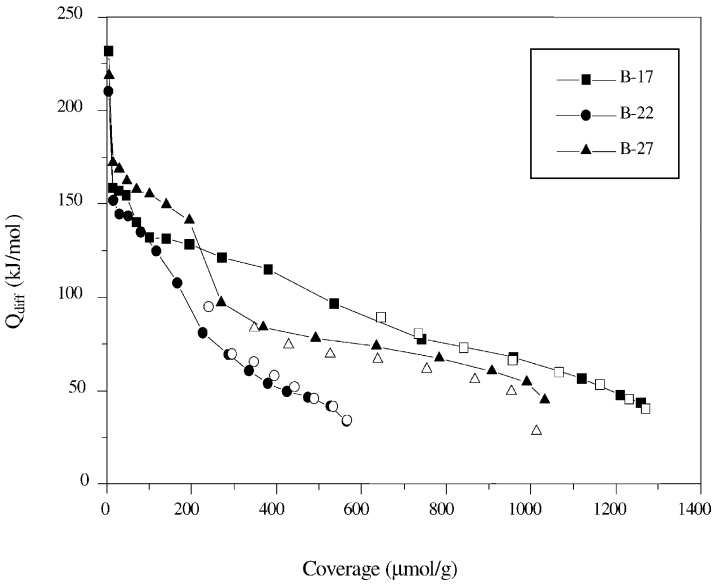

Fig. 2. Differential heats of pyridine adsorption at 423 K as a function of pyridine uptake for beta zeolites. Open symbols refer to readsorption after evacuation.

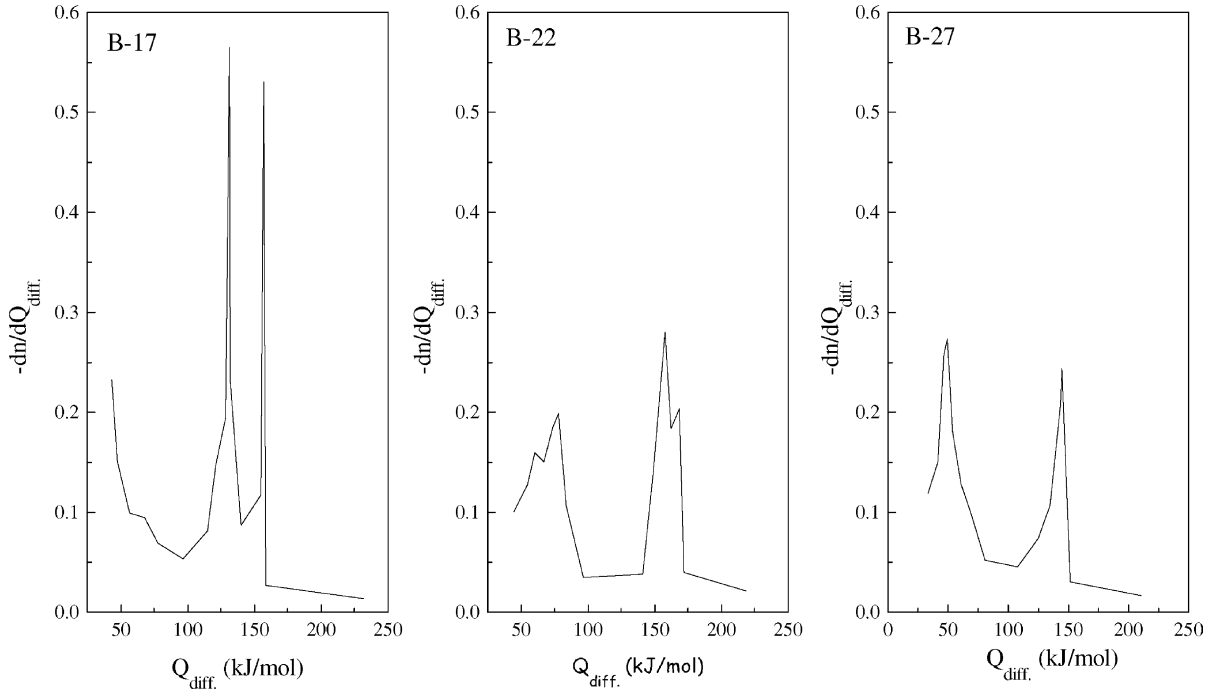

Fig. 3. Site energy distribution plots for beta zeolites, as obtained through graphical derivation of Fig. 2 curves.

In Fig. 4 the total amount of acidic sites estimated through microcalorimetric experiments is compared with the number of Brønsted + Lewis acidic sites assessed by FTIR spectroscopy. The two sets of data are in fair agreement.

3.3. Catalytic activity

The catalytic performance has been expressed as sBB conversion (X_{sBB}, mol%) and selectivity (S, mol%) to the reaction products: *iso*-butylbenzene benzene as ISO product, 1,3- and 1,4-bis-(1-methylpropyl)-benzene as DIS products, and benzene (after subtracting the amount formed through disproportionation) as DEA product. By-products, coming from minor side reactions, were also considered: light alkanes, mainly C_4 (PAR); light alkenes, mainly C_4 (OL); monoalkylated (ALK) and dialkylated benzenes (DIALK) with a molecular weight in the range 92–120 and 148–190 (mainly 1-ethylpropyl-3-ethylbenzene), respectively.

Table 3
Concentration of pyridinium ions ($PyrH^+$: Brønsted acid sites) and of pyridine coordinated to Lewis sites (PyrL: Lewis acid sites) determined by FTIR spectroscopy

Sample	$PyrH^+$ (μmol/g)	PyrL (μmol/g)	$PyrH^+$ + PyrL (μmol/g)
B-17	462	314	776
B-22	413	98	511
B-27	115	97	212

The results for the B-17 catalyst under atmospheric pressure at 573 K are presented first. Fig. 5a shows the vapour phase conversion of sBB as a function of time-on-stream (t.o.s.) at different partial pressures of the reactant (p_{sBB}). Fig. 5b shows the influence of p_{sBB} on the residual activity, X_i/X_f, defined as the ratio between the conversion values at 24 h (X_f) and 1 h (X_i). Whatever the reactant partial pressure, the catalyst deactivates with t.o.s. For the runs where the reactant partial pressure is between 107 and 419 mbar all the data are fitted by the same conversion versus t.o.s. curve. In comparison, the conversion values obtained at $p_{sBB} = 74$ mbar are considerably lower. Under the latter conditions a more pronounced deactivation occurs, clearly indicated by the residual activity values (Fig. 5b).

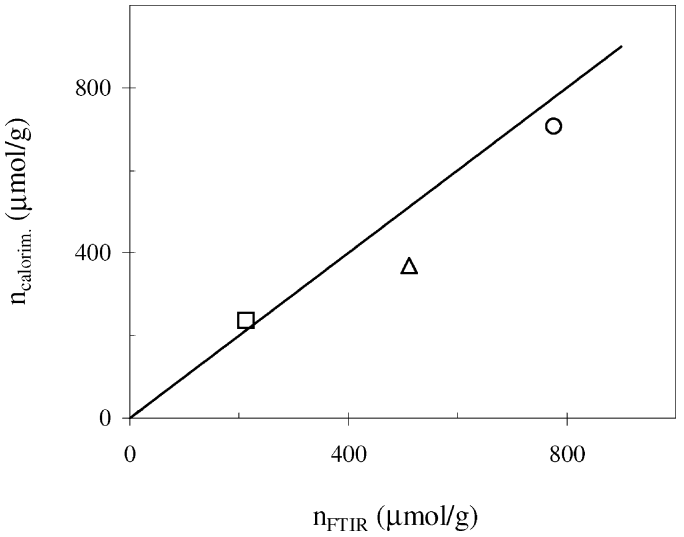

Fig. 4. Comparison of FTIR and microcalorimetric results for beta zeolites. The total concentration of the acid sites estimated by microcalorimetry is plotted vs. the concentration of the Brønsted + Lewis acid sites assessed by FTIR spectroscopy. (○) B-17; (△) B-22; (□) B-27.

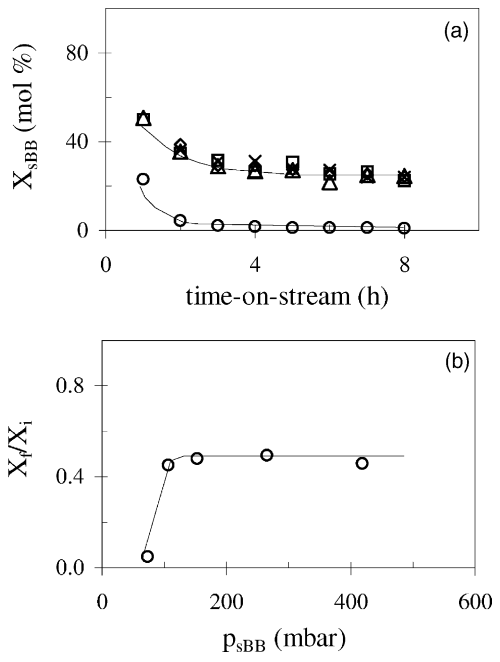

Fig. 5. (a) *sec*-Butylbenzene conversion (X_{sBB}) vs. time-on-stream (a) for B-17 catalyst at 573 K and reactant partial pressure (p_{sBB}) of 74 mbar (○); 107 mbar (□); 153 mbar (△); 265 mbar (◇); and 419 mbar (×). (b) Residual activity (X_f/X_i) as a function of p_{sBB}.

The evolution of DEA, ISO and DIS reactions with t.o.s. at the different reactant partial pressures is shown in Fig. 6a–e. There is no significant influence of p_{sBB} on the initial (1 h on-stream) selectivities for dealkylation, isomerisation and disproportionation, the former reaction being by far predominant in all cases. However, during the run at $p_{sBB} = 74$ mbar dealkylation dramatically decreases while disproportionation increases and becomes predominant at high reaction time. This is not observed for the runs at $p_{sBB} \geq 107$ mbar, where only slight changes in selectivity occur. Concerning the products of the minor reactions, a dramatic increase for ALK and DIALK products with t.o.s. is observed for the run at $p_{sBB} = 74$ mbar (Fig. 7a); by converse, these products decrease during the runs at $p_{sBB} \geq 107$ mbar (Fig. 7b–e). Interestingly, an influence of the reactant partial pressure on the relative amounts of 1,3- and 1,4-bis-(1-methylpropyl)-benzene (*meta* and *para* di-*sec*-butylbenzene formed through disproportionation) was observed. This is shown in Fig. 8, where the *m*/*p* ratio for the two isomers is plotted versus t.o.s. For the runs with $p_{sBB} \geq 107$ mbar the *m*/*p* ratio is 2.2 at any t.o.s.; for the run at $p_{sBB} = 74$ mbar the *m*/*p* ratio decreases as t.o.s. increases, dropping from 2.2 to 1.3 after 8 h reaction.

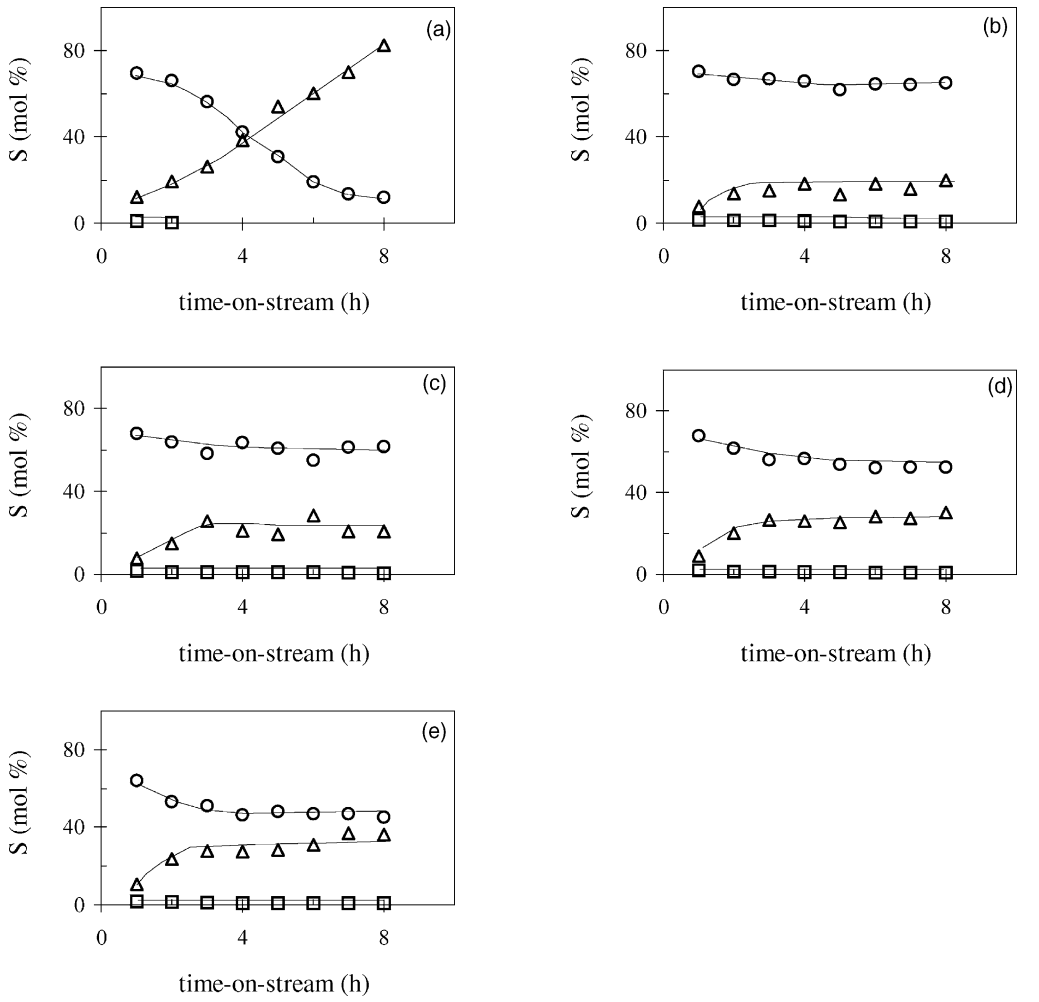

Fig. 6. Selectivities (*S*) to DEA (○), ISO (□) and DIS (△) products vs. time-on-stream for B-17 catalyst at 573 K and reactant partial pressure (p_{sBB}) of 74 mbar (a); 107 mbar (b); 153 mbar (c); 265 mbar (d); and 419 mbar (e).

The catalytic behaviour of B-17 sample in the liquid-phase transformation of sBB under 40 bar pressure and 573 K is summarised in Figs. 9–11. Comparison of Fig. 9 with Fig. 5a shows that the initial conversion in the liquid-phase is higher than that for the vapour phase at $p_{sBB} \geq 107$ mbar; a smoother decreasing trend is observed in the liquid-phase as t.o.s. increases. The selectivities for DEA, ISO and DIS reactions are plotted versus t.o.s. in Fig. 10. The isomerisation extent in liquid-phase is significantly higher than in vapour phase (cf. Fig. 10 with Fig. 6). While disproportionation markedly increases, isomerisation decreases very slightly with t.o.s. A remarkable decreasing trend is observed for dealkylation. The *m*/*p* ratio for the di-*sec*-butylbenzene isomers was found to be higher than 2 and constant over the whole reaction time. The selectivity towards PAR, ALK, DIALK and TRIALK products changes with t.o.s. as shown in Fig. 11. No olefinic hydrocarbons were detected in the runs at 40 bar, which is at variance with the case of vapour phase reaction.

The influence of the reaction temperature on the initial conversion and residual activity of the catalyst at both atmospheric pressure (vapour phase,

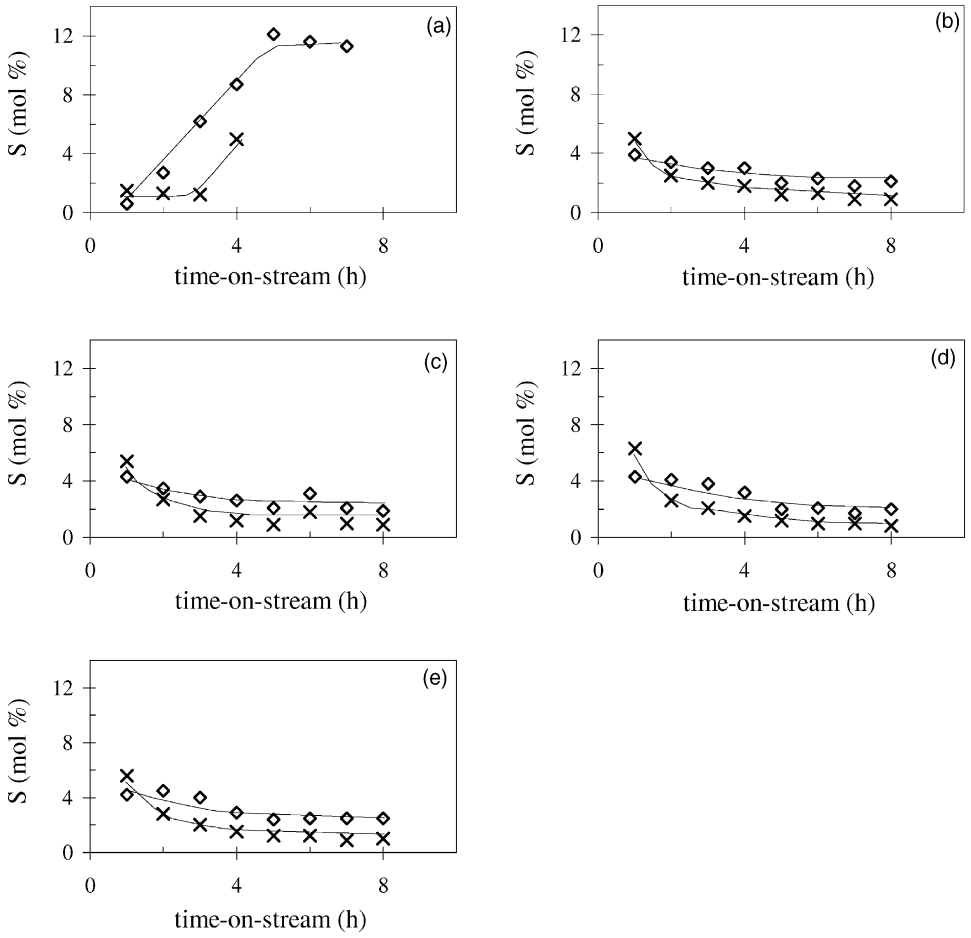

Fig. 7. Selectivities (S) to ALK (×) and DIALK (◇) products vs. time-on-stream for B-17 catalyst at 573 K and reactant partial pressure (p_{sBB}) of 74 mbar (a); 107 mbar (b); 153 mbar (c); 265 mbar (d); and 419 mbar (e).

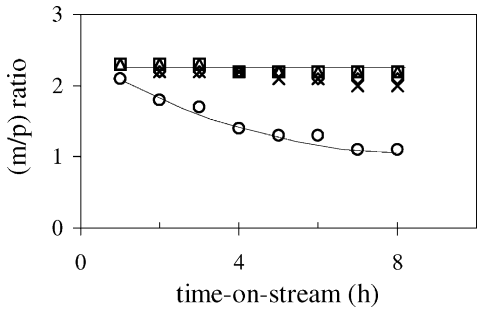

Fig. 8. A *meta*/*para* (m/p) ratio between the two di-*sec*-butylbenzene isomers vs. time-on-stream for B-17 catalyst at 573 K and reactant partial pressure (p_{sBB}) of 74 mbar (○); 107 mbar (□); 153 mbar (△); 265 mbar (◇); and 419 mbar (×).

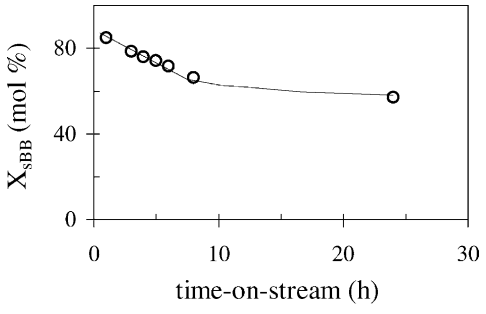

Fig. 9. *sec*-Butylbenzene conversion (X_{sBB}) in liquid phase ($p = 40$ bar) vs. time-on-stream for B-17 catalyst at 573 K.

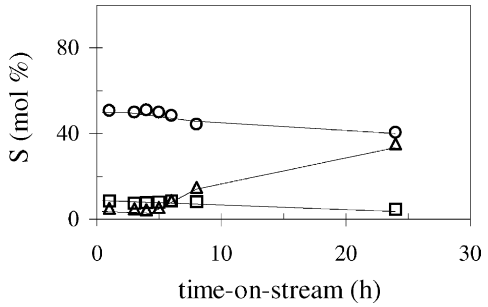

Fig. 10. Selectivities (*S*) to DEA (○), ISO (□) and DIS (△) products in liquid phase ($p = 40$ bar) vs. time-on-stream for B-17 catalyst at 573 K.

$p_{sBB} = 107$ mbar) and 40 bar (liquid-phase), is shown in Fig. 12. An increase in temperature enhances conversion and lowers the residual activity. Products distribution of the sBB transformation as a function of the reaction temperature under atmospheric and 40 bar pressure is presented in Table 4. In vapour phase operation higher temperatures favour dealkylation, mostly at the expense of disproportionation; a simultaneous decrease in isomerisation also occurs. Olefins formation markedly increases with the reaction temperature; paraffins, detected in trace amounts at 473 K, form to some extent at 523 and 573 K. ALK and DIALK products show opposite trends: the former increase and the latter decrease upon increasing the reaction temperature. A similar influence of temperature on the competing DEA, DIS, and ISO reactions is observed in liquid-phase. Olefins and paraffins are simultaneously present at 523 K; no paraffins are detected at 473 K, while no olefins are present at 573 K.

Table 4
Products distribution (in %) at different reaction temperatures, under 1 and 40 bar pressure, for B-17 catalyst

	T (K)					
	473		523		573	
	1 bar	40 bar	1 bar	40 bar	1 bar	40 bar
PAR	0.5	0.3	2.5	2	1.7	22
OL	0.9	7	5.5	11	8.8	–
DEA	30	25	57.7	40.4	70.4	50.8
DIS	46.2	27	20.2	20	7.3	5
ISO	15	22	5.4	12	1.8	8.4
ALK	1	2.5	3.7	3.6	6	6.6
DIALK	6.4	16.2	5	11	4	7.2

The catalytic behaviour of B-17 has been compared with that of B-22 and B-27 samples at 473 K under atmospheric pressure ($p_{sBB} = 107$ mbar). A plot of conversion versus t.o.s. for the three catalysts is shown in Fig. 13. A remarkable difference in the conversion level is observed between B-17 and B-22 on the one side and B-27 on the other. The evolution of DEA, ISO and DIS selectivities with t.o.s are shown in Fig. 14a–c, respectively. The trends are similar for the three catalysts: DEA selectivity drops after few hours on-stream, a smoother decrease occurs for ISO, DEA suddenly grows and attains a plateau. Disproportionation is by far predominant at any t.o.s. Fig. 15 shows that no changes in the *m*/*p*-di-*sec*-butylbenzene occur during the run for any of the catalysts.

4. Discussion

Dealkylation, disproportionation and isomerisation of alkylaromatics are acid catalysed reactions involving as a first step the formation of a σ-adduct on a surface protonic site. It is the fate of the σ-adduct that determines which reaction takes then place. In the case of dealkylation, C–C bond rupture occurs, leading to the formation of a benzene molecule and an alkylcarbenium ion. This is sketched for *sec*-butylbenzene in Scheme 1, where the CH_3–CH^+–CH_2–CH_3 (C_4^+) ion is shown to evolve towards 2-butene and/or *iso*-butane. Besides, the C_4^+ ion can be also involved in other reactions, such as dimerisation to C_8, which, by β-scission, gives C_3 and C_5 fragments. From the latter a variety of products can be originated, including variously alkylated compounds. Oligomerisation can be also followed by cyclisation and lead to other aromatics. Furthermore, oligomerisation giving high molecular weight products represents a step towards coke formation.

The occurrence of isomerisation requires, at variance with the case of dealkylation, that the σ-adduct undergoes an internal rearrangement with formation of a benzylic ion. It should be noted however that such a benzylic ion might also form directly through intermolecular hydrogen transfer between *sec*-butylbenzene and a carbenium ion (e.g. C_4^+ coming from sBB dealkylation), thus by-passing

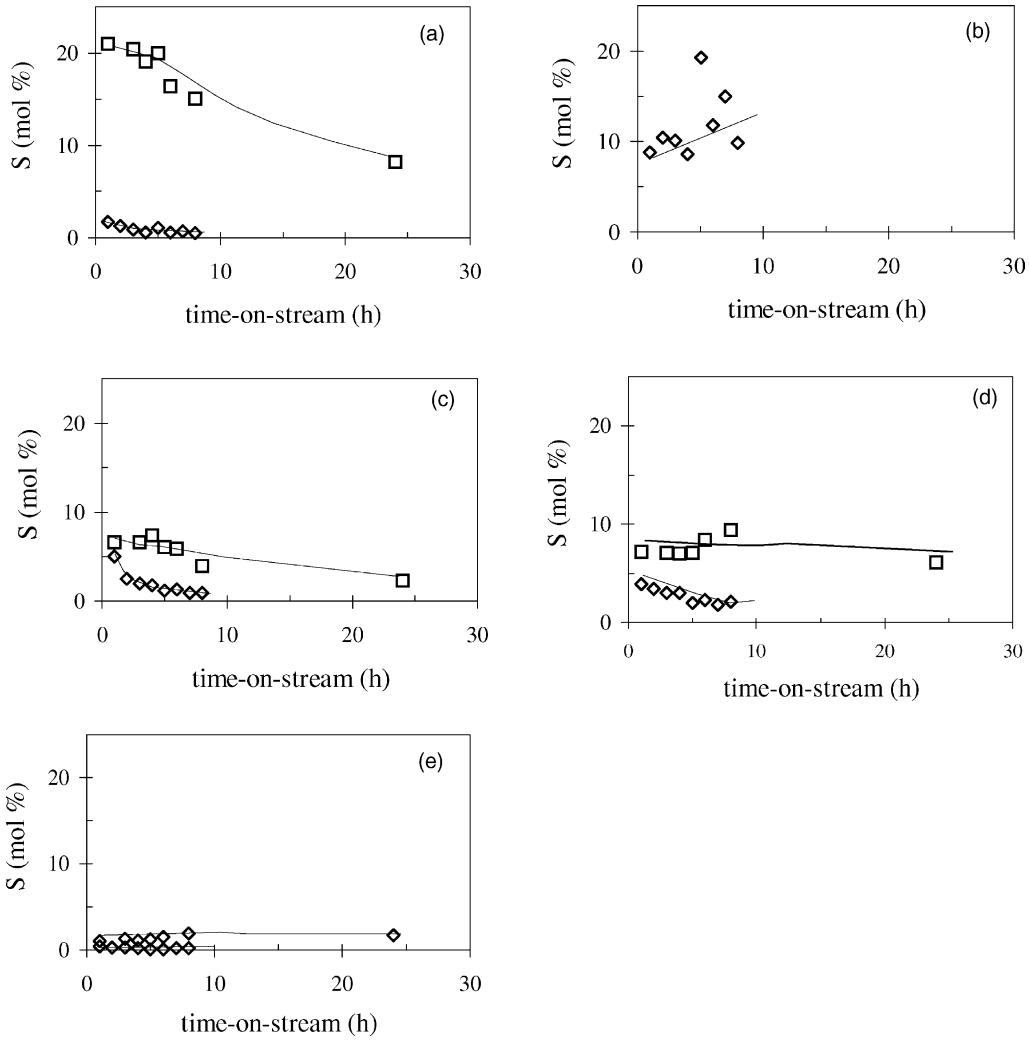

Fig. 11. Selectivities (*S*) to minor products: PAR (a), OL (b), ALK (c), DIALK (d) and TRIALK (e) in gas-phase (◇) and in liquid-phase (□) vs. time-on-stream for B-17 catalyst at 573 K.

the σ-adduct formation step. Both these possibilities for *iso*-butylbenzene formation are shown in Scheme 2.

Benzylic ions, either originated from the σ-adduct or formed directly by interaction of sBB with C_4^+ (or other R^+) ions are also involved in the disproportionation mechanism. According to many authors [7,8,19–22] this reaction could take place with either an S_N1 or an S_N2 mechanism, depending on the available space within the porous system of the zeolite, as well as on the reaction conditions. The S_N2 mechanism (Scheme 3) involves the intervention of two sBB molecules, with formation of a diphenylalkane intermediate. From the latter, benzene and di-secbutylbenzene are formed. The dialkylated product is a mixture of the *m*- and *p*-isomers. According to the calculated values [7] of the electronic charge on the *ortho*, *meta* and *para* positions, attack on the *meta* position should be favoured. In the case of steric constraints, i.e. for zeolites of low

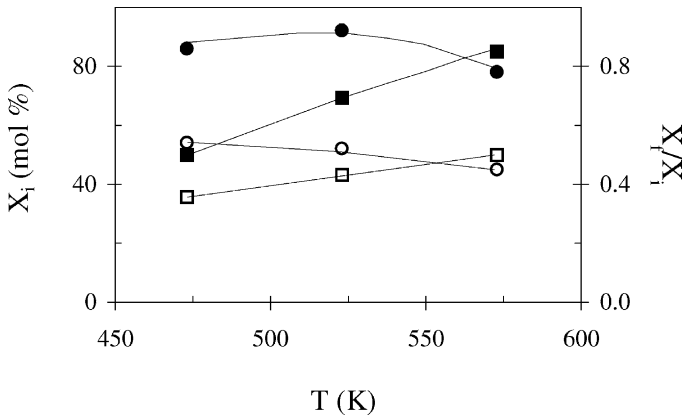

Fig. 12. Influence of the reaction temperature on the initial conversion (X_i) (squares) and residual activity (X_f/X_i) (circles) for B-17 catalyst vs. reaction temperature. Open symbols refer to 1 bar, full symbols to 40 bar pressure.

spaciousness index and/or coke formation, disproportionation occurs through a monomolecular (S_N1) mechanism (Scheme 4). This involves the dealkylation of a molecule of *sec*-butylbenzene with formation of a carbenium ion, which alkylates another sBB molecule giving the dialkylated product. The *m*/*p* ratio between the two dialkylated isomers gives an indication about the relative extent of the S_N2 and S_NI mechanisms. An *m*/*p* ratio $\geq$ 2 indicates that the disproportionation mechanism is mainly of S_N2 type [7,20]. The *meta*/*para* ratios of 1.3-1.5 [8] or lower (0.3 for ZSM-5 zeolites [20]) have been reported in concomitance with S_N1 mechanism. An outline of the reaction pathways for the conversion of *sec*-butylbenzene, based on the products distribution experimentally observed in a former [7] as well as in the present work is presented in Scheme 5.

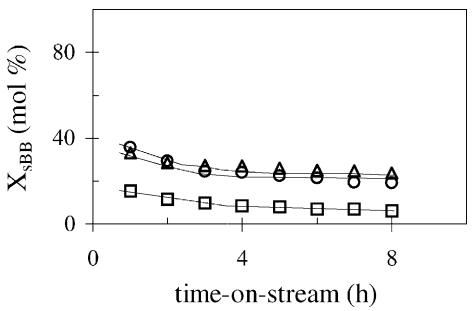

Fig. 13. *sec*-Butylbenzene conversion (X_{sBB}) vs. time-on-stream, at 1 bar and 473 K, for B-17 (○), B-22 (△) and B-27 (□) catalysts.

This general picture allows to discuss the behaviour of the B-17 catalyst. In vapour phase there is no beneficial effect in operating at reactant partial pressures higher than 107 mbar, neither in conversion (Fig. 5a) nor in stability terms (Fig. 5b). Such a partial pressure value seems to be the threshold beyond which all the active sites are permanently (in a dynamic way) occupied by adsorbed reactant molecules. The activity decay is obviously related to the occurrence of coking. Deactivation occurs faster (and leads to a very low residual activity) at $p_{sBB} = 74$ mbar than at $p_{sBB} \geq 107$ mbar (Fig. 5a and b). This seems to indicate a higher toxicity of coke in the former case, in spite of the lower initial conversion. Note that the dramatic activity decay during the run at $p_{sBB} = 74$ mbar is accompanied by an inversion of selectivity from dealkylation to disproportionation (Fig. 6a). Simultaneously, the mechanism of the latter reaction shifts from S_N2 to S_N1, as indicated by the decreasing trend of the *m*/*p*-di-*sec*-butylbenzene ratio with t.o.s. (Fig. 8). Apparently, a dramatic decrease in the available space within the pore system occurs, due to coke deposition; as a consequence, the bimolecular mechanism requiring the formation of the cumbersome diphenylalkane intermediate (Scheme 3) no longer takes place and the monomolecular mechanism sets in.

It might be tempting to conclude from the above that during the low conversion run coke deposition leads to pore blockage since the early hours on-stream. The access to the relatively large voids at channel intersections would be soon hindered and most of the

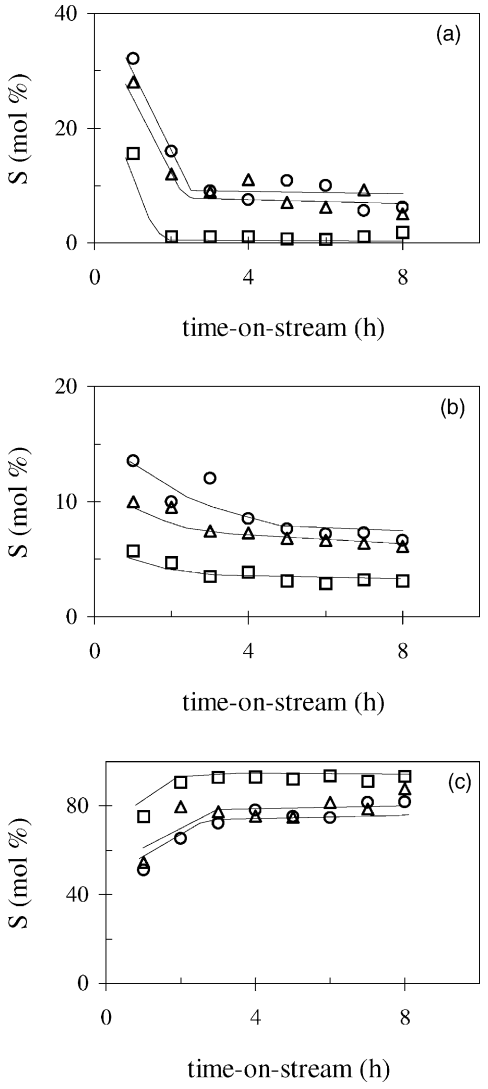

Fig. 14. Selectivities (*S*) to DEA (a), ISO (b) and DIS (c) products vs. time-on-stream, at 1 bar and 473 K, for B-17 (○), B-22 (△) and B-27 (□) catalysts.

active sites would be no more able to interact with the reactant (fast deactivation). The residual activity, now occurring in the confined space of pores rather than at channel intersections, would be governed by the less space-demanding (dealkylation–realkylation) mechanism. Furthermore, severe hindrance in the diffusion of the reaction products would also be expected. This would also favour consecutive realkylation of primary benzene (coming from either DEA or DIS) by C_3 and C_5 fragments and might explain the remarkable increase of other alkylaromatics (DIALK and ALK) with t.o.s. (Fig. 7a).

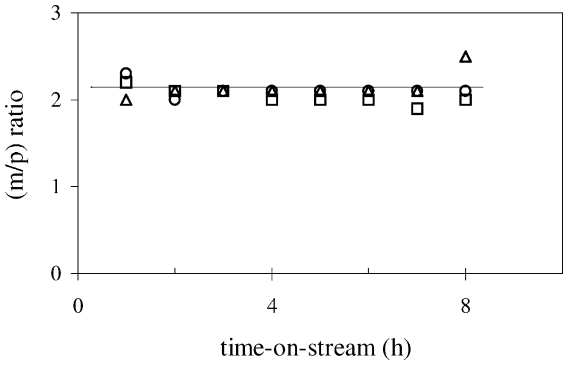

Fig. 15. A *meta*/*para* (*m*/*p*) ratio between the two di-*sec*-butylbenzene isomers vs. time-on-stream, at 1 bar and 473 K, for B-17 (○), B-22 (△) and B-27 (□) catalysts.

Neither inversion between DEA and DIS selectivity (Fig. 6b–e) nor shifting from S_N2 to S_N1 mechanism (as indicated by the *m*/*p*-di-*sec*-butylbenzene ratio in Fig. 8) occurs during the runs carried out at $p_{sBB} \geq 107$ mbar, for which the initial conversion is relatively high. This suggests that, in spite of coke deposition, enough space is still available within the porous system for allowing the persistence of the bimolecular mechanism. Note also that DIALK and ALK products do not grow with t.o.s. (Fig. 7b–e). It might be speculated, also on the basis of the relatively mild deactivation (in comparison with the run at $p_{sBB} = 74$ mbar, Fig. 5a and b), that no pore blockage occurs during these runs; rather, the coke would form inside the channel intersections.

An influence of the reaction severity on the location of carbonaceous material has been reported [23] for ethylbenzene disproportionation over beta zeolites. A 25–45% conversion level was attained at 573 K and 333 mbar; the retained material did not contain "soft" coke and the preferred location was suggested to be at the windows near the channel intersections. The operating conditions make possible a comparison with those among the present runs where p_{sBB} is in the range 107–419 mbar ($T = 573$ K, conversion = 50–25%). It is worthy of note that the location of coke suggested in [23] (for 25–45% conversion) and the conclusion stemming from the present results (for 50–25% conversion) are quite in agreement, in spite of

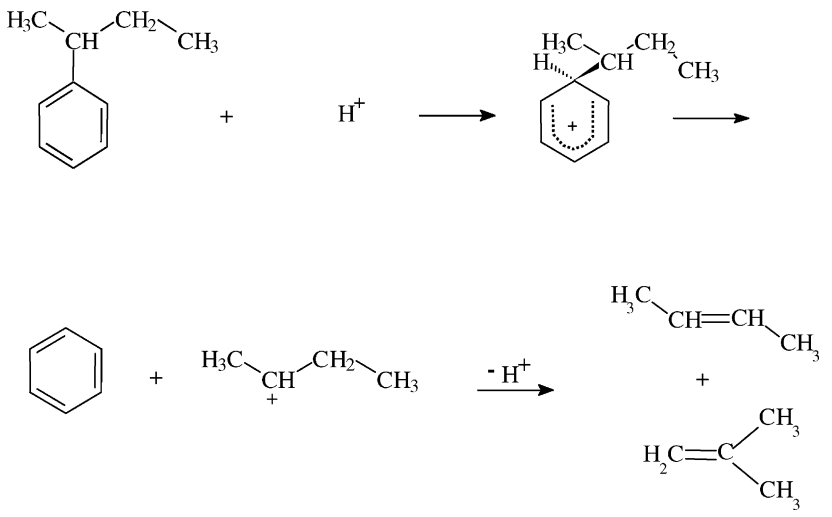

Scheme 1. Dealkylation.

different reactant nature. Obviously, the tentative hypothesis earlier outlined for the location of coke during *sec*-butylbenzene transformation over B-17 zeolite needs further experimental evidence. The assessment of the amount and nature of coke by means of suitable analytical tools [24] is expected to give clues in this direction and will form the subject of a forthcoming development of the present work.

The remarkable increase in both conversion and stability of B-17 in liquid-phase as compared to vapour phase operation (cf. Fig. 9 with Fig. 5) can be ascribed to the dissolution/extraction by the liquid reactant of the coke precursors, whose growth towards bulkier polyaromatic material is hence avoided. The lack of olefins, well-known intermediates in coke-forming reactions, could play a significant role as well. As expected, fragmentation reactions such as dealkylation are significantly depressed by operation under high pressure (cf. Fig. 10 with Fig. 6). The on-stream behaviour seems to indicate no pore

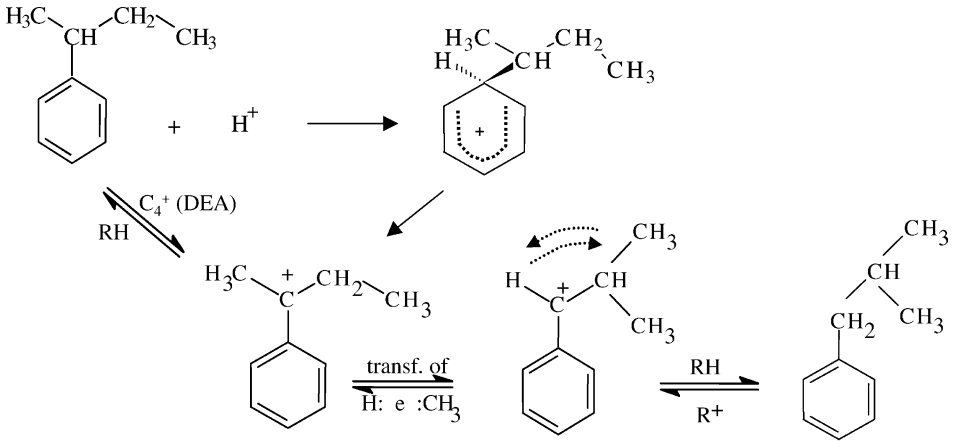

$R^+ = C_4^+$ (DEA) or benzilic carbocation

Scheme 2. Isomerisation.

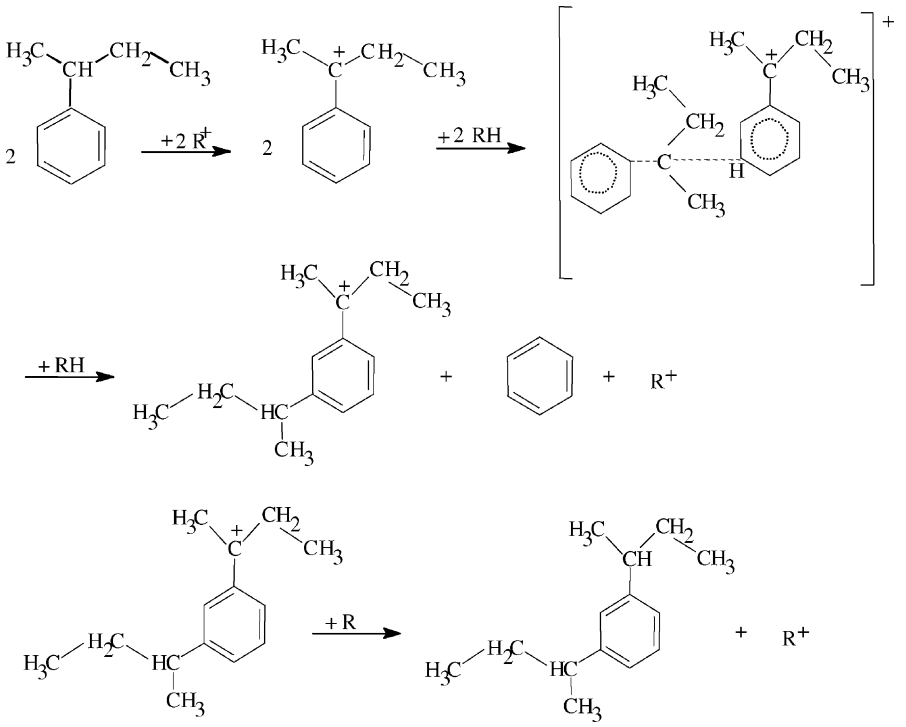

Scheme 3. Disproportionation: S_N2 mechanism.

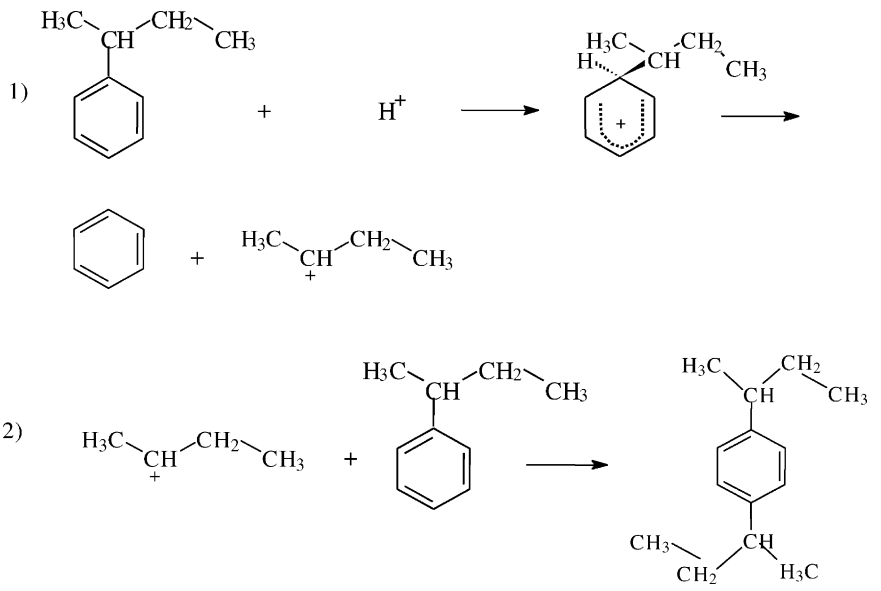

Scheme 4. Disproportionation: S_N1 mechanism.

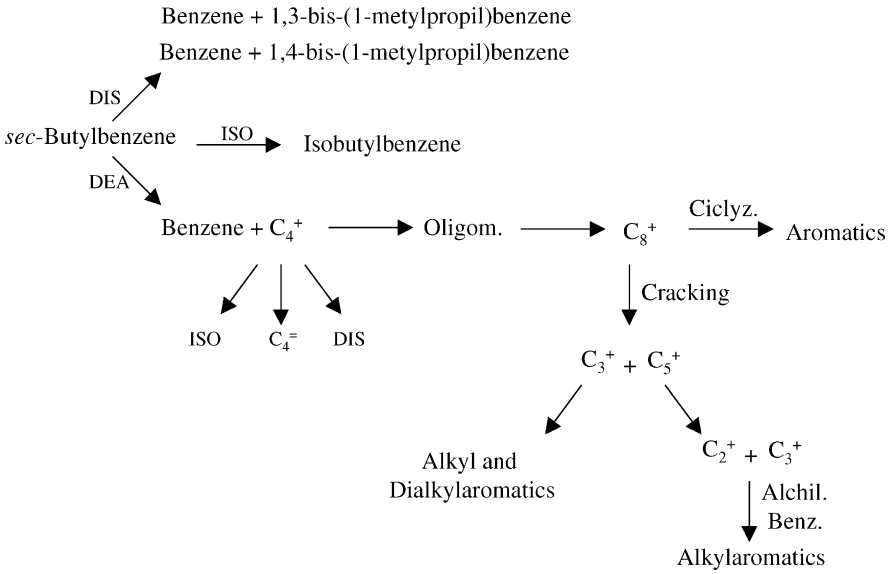

Scheme 5. Reaction pathways for the conversion of *sec*-butylbenzene.

blockage by coke during liquid-phase operation: deactivation is relatively mild (even milder than that in vapour phase at $p_{sBB} \geq 107$ mbar, for which no pore blockage was observed); bimolecular S_N2 mechanism persists even at the highest reaction time (*m*/*p*-di-*sec*-butylbenzene ratio = 2 at any t.o.s. value), i.e. there is always enough space available inside the pore system for allowing the formation of the diphenylalkane intermediate. Coke deposition affects the dealkylation and disproportionation selectivities in such a way that a dramatic increase (from ca. 5 to 35%) in the latter occurs simultaneously with a decrease in dealkylation (Fig. 10). No increase in the ALK, DIALK and TRIALK curves is observed (Fig. 11) in concomitance with the establishing of the decreasing trend for the DEA (Fig. 10) and PAR (Fig. 11) curves. Accordingly, a decrease in the dealkylation products (benzene and C_4) due to their involvement in successive realkylation reactions should be ruled out, which is also consistent with the finding that the dealkylation–realkylation mechanism for disproportionation does not set in during run.

The observed trends for DEA, ISO and DIS appear somewhat puzzling at first sight. The decrease in dealkylation should entrain a decrease in the amount of C_4^+ (or other R^+) ions available for triggering isomerisation and disproportionation throngh the consecutive pathway sketched in Scheme 5.

Disproportionation, which is bimolecular (Scheme 3), should be more sensitive to the concentration of these ions than isomerisation. As a consequence, the DEA-to-(DIS + ISO) ratio should not change with t.o.s., while a decrease in the DIS-to-ISO ratio should be expected, which is at variance with the experimental findings. To explain the latter it could be tentatively suggested that: (i), at the early hours on-stream the DEA products are largely formed through secondary dealkylation (i.e. occurring on the isomerisation and disproportionation products); (ii), during the run progressive poisoning of the stronger acid sites by coke occurs, mainly affecting the extent of secondary dealkylation. Should this occur, an increasingly higher amount of DIS products would be found in the reactor effluent, which would account for the observed increasing trend of DIS selectivity (and the decrease in DEA selectivity as well). Such a role of the strong acid sites in promoting secondary dealkylation seems reasonable. The competition between isomerisation and disproportionation, on the one side, and primary dealkylation (i.e. occurring on the reactant sBB only), on the other, would depend on the extent to which σ-adduct undergoes rearrangement (giving isomerisation and disproportionation products) instead of C–C

bond rupture (giving primary dealkylation). There is no reason for which the presence of strong sites would favour the latter over the former pathway. (Due to the higher activation energy of C–C bond rupture in comparison with the rearrangement, a major role should be played by the reaction temperature). However, on the stronger sites it would be more difficult for the rearranged ions to release a proton (due to the weaker character of the conjugated base site) to give the ISO and DEA products; this would increase the residence time on the surface of the rearranged ions, which would have a higher chance to undergo C–C bond rupture (secondary dealkylation).

By comparing the results for B-17, B-22 and B-27 samples in vapour phase at 473 K an influence of acidity on the catalytic behaviour is manifest. Fig. 16 shows the influence of the Brønsted acidity (from Table 3) of the catalysts and their initial conversion (at 1 h on-stream, from Fig. 13). As the concentration of Lewis sites on B-22 and B-27 is the same (Table 3), it can be assumed that the acid-strength distribution for these two samples reported in Table 2 reflects that of their Brønsted sites. B-22, which has a higher concentration of strong acid sites (238 μmol/g) than B-27 (95 μmol/g), has a higher dealkylating character (Fig. 14a). However, it is worthy of note that, in spite of its very high concentration of strong sites, B-22 is more a DIS than a DEA catalyst (cf. Fig. 14c with Fig. 14a). This seems to support the view that the strong acid sites do not simply favour primary dealkylation over the competing disproportionation and isomerisation (i.e. C–C bond rupture in the σ-adduct, instead of its rearrangement); rather, they strongly retain the rearranged ions, hence favouring their successive dealkylation. For none of the catalysts the pore volume seems significantly altered by coke deposition (disproportionation occurs through the S_N2 mechanism, whatever the t.o.s. value, Fig. 15). The observed activity decay (Fig. 13) would result form poisoning of the sites. The selectivity trends in Fig. 14 seem in agreement with the proposed role for the strong sites: their rapid poisoning entrains a decrease in the extent of secondary dealkylation and a simultaneous increase in disproportionation.

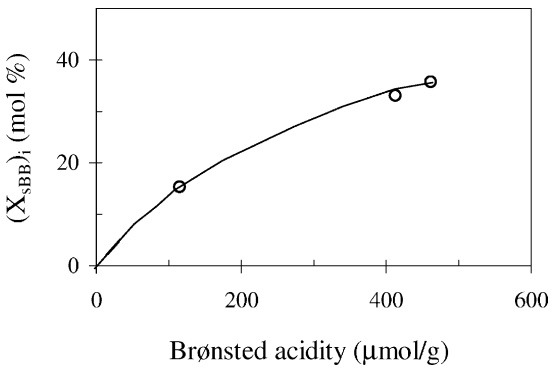

Fig. 16. Influence of initial (1 h on-stream) conversion of *sec*-butylbenzene $(X_{sBB})_i$ on the Brønsted acidity of the beta zeolites.

5. Conclusions

The conversion of *sec*-butylbenzene over H-beta zeolite catalysts is a complex process involving many steps, the main reactions being dealkylation, isomerisation and disproportionation, depending on the concentration and strenght of the catalyst and on the reaction conditions. Many different products, come from these reactions: primary products, including benzene, *iso*-butylbenzene, di-*sec*-butylbenzenes, butenes and isobutenes, and secondary products, including butane, *iso*-butane, toluene, xylenes, ethylbenzene, propylbenzene and the carbonaceous compounds referred to as coke.

At 1 bar (vapour phase), the catalyst deactivation is faster than at 40 bar (liquid-phase) due to polymerisation and cyclisation of light alkenes and/or to condensation of polyalkylbenzenes, leading to coke. Operating in liquid-phase has a very positive effect on the life and stability of the catalyst: light olefins, well-known as coke precursors, are absent and the hot-spots on the catalyst surface are damped down because of the presence of the liquid reactant, which is also able to dissolve the coke precursors and to clean up continuously the catalyst surface.

Whatever the reactant partial pressure ($74 < p_{sBB} < 419$ mbar), the catalyst deactivates with time-on-stream. The activity decay is obviously related to the occurrence of coking. Deactivation occurs faster at $p_{sBB} < 107$ mbar due to the higher toxicity of coke. The coke plays a role totally different depending on the reaction severity. At low conversion ($p_{sBB} = 74$ mbar), the coke deposition leads to pore blockage, while at high conversions ($p_{sBB} = 107$–419 mbar),

the coke would form inside the channel intersections leading to a mild deactivation, without pore blockage.

References

[1] M.M.J. Treacy, J.M. Newsam, Nature 332 (1988) 249.
[2] J.B. Higgins, R.B. LaPierre, J.L. Schlenker, A.C. Rohrman, J.D. Wood, G.T. Kerr, W.J. Rohrbaugh, Zeolites 8 (1988) 446.
[3] R. Benslama, J. Fraissard, A. Albizane, F. Fajula, F. Figueras, Zeolites 8 (1988) 196.
[4] R.L. Wadlinger, G.T. Kerr, E. Rosinski, US Patent 3,308,069 (1967) and reissued US Patent 28,341 (1975).
[5] L. Bonetto, M.A. Camblor, A. Corma, J. Pérez-Pariente, Appl. Catal. A: Gen. 82 (1992) 37.
[6] J.A. Rabo, Zeolite chemistry and catalysis, ACS Monogr. 171 (1976) 437.
[7] P. Artizzu, R. Monaci, E. Rombi, I. Ferino, V. Solinas, L. Forni, Appl. Catal. A: Gen. 111 (1994) 191.
[8] E. Rombi, R. Monaci, M. Muscas, I. Ferino, V. Solinas, L. Forni, in: H.K. Beyer, H.G. Karge, I. Kiricsi and J.B. Nagy (Eds.), Catalysis by Microporous Materials, Study of Surface Science and Catalysis, vol. 94, Elsevier, Amsterdam, 1997, p. 1.
[9] H. Szmant, Organic Building Blocks of the Chemical Industry, Wiley, New York, 1989, p. 529.
[10] R.L. Wadlinger, G.T. Ken, E.J. Rosinski, US Patent 3,308,069 (1967).
[11] R.J. Argauer, G.R. Landolt, US Patent 3,702,886 (1972).
[12] V. Solinas, I. Ferino, Catal. Today 41 (1998) 179.
[13] C. Coutanceau, J.M. Da Silva, M.F. Alvarez, F.R. Ribeiro, M. Guisnet, J. Chem. Phys. 94 (1997) 765.
[14] G. Horvath, K. Kawazoe, J. Chem. Eng. Jpn. 16 (6) (1983) 470.
[15] D.A. Payne, K.S.W. Sing, J. Coll. Interf. Sci. 43 (1973) 287.
[16] W.D. Harkins, G. Jura, J. Chem. Phys. 11 (1943) 431.
[17] M. Brotas de Carvalho, A.P. Carvalho, F.R. Ribeiro, A. Florentino, N.S. Gnep, M. Guisnet, Zeolites 14 (1994) 217.
[18] I. Ferino, R. Monaci, E. Rombi, V. Solinas, P. Magnoux, M. Guisnet, Appl. Catal. A: Gen. 183 (1999) 303.
[19] K. Itoh, G. Yamada, S. Hamanaka, M. Ogawa, Bull. Chem. Soc. Jpn. 41 (1968) 2504.
[20] T.C. Tsai, I. Wang, J. Catal. 133 (1992) 136.
[21] W.W. Kaeding, J. Catal. 120 (1989) 409.
[22] A. Corma, V. Fornés, J. Perez-Pariente, E. Sastre, J.A. Martens, P.A. Jacobs, in: W.H. Flank, T.E. White (Eds.), Proceedings of the ACS Symposium Series on Perspectives in Molecular Sieve Science, vol. 368, 1988, p. 555.
[23] A.R. Pradhan, J.F. Wu, S.J. Jong, W.H. Chen, T.C. Tsai, S.B. Liu, Appl. Catal. A: Gen. 159 (1997) 187.
[24] P. Magnoux, P. Roger, C. Canaff, V. Fouché, N.S. Gnep, M. Guisnet, Study of Surface Science and Catalysis, vol. 34, Elsevier Amsterdam, 1987, p. 317